Progress In Electromagnetics Research, Vol. 144, 151–169, 2014

The Wavelength Division Multiplexer Realized in Three-Dimensional Unusual Surface-Plasmon-Induced Photonic Crystals Composed of the Epsilon-negative Materials Shells

Hai-Feng Zhang[1, 2, 3, *], Shao-Bin Liu[1, 3], and Hai-Ming Li[1, 3]

Abstract—In this paper, the dispersive properties and switching state of three-dimensional (3D) photonic crystals (PCs) with diamond lattices, which are composed of the core isotropic dielectric spheres with surrounded by the epsilon-negative (ENG) materials shells inserted in the isotropic dielectric background (air), are theoretically investigated in detail based on a modified plane wave expansion method. The wavelength division multiplexer can be realized easily by tuning the switching state of such PCs. The equations for computing band structures for such 3D PCs are presented. Our analysis shows that the proposed double-shell structures can obtain the complete photonic band gaps (PBGs) which can be used to realize optical switching by manipulating the radius of core dielectric sphere, the relative dielectric constant of background, the dielectric constant of ENG materials and the electronic plasma frequency, respectively. However, the thickness of the ENG materials shell cannot change the switching state as the radius of core dielectric sphere is certain. Numerical simulations also show that a flatband region, and the stop band gaps (SBGs) in (1 0 0) and (1 1 1) directions which are above the flatband region can be achieved. The SBGs in (1 0 0) and (1 1 1) directions can also be tuned by the parameters as mentioned above. There also exists a threshold value for the thickness of ENG material shell, which can make the band structures for the 3D PCs with double-shell structures similar to those obtained from the same structure containing the pure ENG materials spheres. In this case, the inserted core sphere will not affect the band structures. It means that we can achieve the PBGs by replacing the pure ENG materials spheres by such double-shell structures to make fabricate easily and save the material in the realization. It is also noticed that the flatband region is determined by the existence of surface-plasmon modes, and the upper edge of flatband region does not depend on the topology of lattice. Such presented 3D PCs with double-shell structures offer a novel way to realize the wavelength division multiplexers.

1. INTRODUCTION

The idea of photonic crystals (PCs) is first proposed by Yablonovitch [1] and John [2], which are a kind of artificial materials with periodic arrangement of different dielectrics in space. The PCs have attracted great attention from researchers due to their abilities to produce the photonic band gaps (PBGs) [3]. If the frequency of electromagnetic (EM) wave is located in such magic regions, any polarizations of EM waves cannot propagate through PCs along any directions. This unique feature makes PCs used as a promising candidate to build many important optical devices, such as absorber [4], all-optical adder [5], filter [6], omnidirectional reflector [7], and waveguide [8]. During last two decades, the optical properties of PCs have been studied extensively. However, the conventional dielectric PCs are highly sensitive to the lattices and randomness when they are worked as the optical devices. It

Received 1 November 2013, Accepted 23 December 2013, Scheduled 15 January 2014

* Corresponding author: Hai-Feng Zhang (hanlor@163.com).

[1] College of Electronic and Information Engineering, Nanjing University of Aeronautics and Astronautics, Nanjing 210016, China. [2] Nanjing Artillery Academy, Nanjing 211132, China. [3] Key Laboratory of Radar Imaging and Microwave Photonics, Ministry of Education, College of Electronic and Information Engineering, Nanjing University of Aeronautics and Astronautics, Nanjing 210016, China.

means that the PBGs not only suffer from the errors from manufacturing, but also cannot be tuned as the constituents and topologies of PCs are certain. To overcome such drawbacks, metamaterials are introduced into the conventional PCs to obtain the tunable PBGs [9–11]. Metamaterials are firstly proposed theoretically by Veselago in 1968 [12], which can also be called left-hand materials due to their unusual physical properties such as inverse Snell's law, negative refraction index, Cherenkov effects and reversed Doppler effect. Recently, metamaterials have been realized in experiment by Simth et al. [13] and Pendry [14], and also investigated extensively. Morits and Simovski [15] studied the EM properties of planar and bulk metamaterials in theory and found that the scattering parameters of bilayer metafilm can be predicted by the proposed method. Simth et al. [16] also demonstrated that the effective permittivity and permeability of finite lengths of metamaterials can be obtained successfully by the transmission/reflection coefficients computed from transfer matrix simulations. Liu and Alu [17] realized the zero-index or quasi-isotropic negative-index metamaterials in a certain frequency region with negligible dispersive effects by a metamaterial geometry composed of periodic arrays of densely magnetodielectric spheres. Holloway et al. [18] derived a model for the reflection and transmission properties of a metafilm by using generalized sheet transition conditions, and they found that the coefficients of transmission and reflection for metafilm can be expressed in term of the magnetic and electric polarizabilities of the scatterers on the metafilm as the incident plane wave is arbitrary. Kim et al. [19] presented line-reflect-line-like expressions for obtaining the parameters of a metamaterial by the measuring the S-parameters but do not need any information interior to the metamaterial, and they also found that the boundary effects and spatial dispersion will be observed in a metamaterial. Dimitriadis et al. [20] developed a accurate matrix surface susceptibility model for the homogenization of metasurfaces under oblique TE plane wave incidence, and they proclaimed that the efficiency of the model is contingent upon the electrical size of the scatterers rather than the lattice periodicity. Epsilon-negative (ENG) materials can be looked as a kind of metamaterials [9–11], in which permittivity ε is negative, but permeability μ is positive. However, if μ and ε are negative, the double-negative (DNG) metamaterial can be obtained. As mentioned in the report by Penciu et al. [21], the DNG metamaterial can be realized by coupled split-ring resonators, and multi-gaps can also be obtained. Sounas et al. [22] investigated the optimal design of arbitrarily-dimensional DNG metamaterial slabs and the focusing characteristic based on the a new technique, which employs the signal processing notions of the cross-correlation coefficient, and mean square error is introduced. Compared to the DNG metamaterial, the ENG materials can always be found in nature and can also be obtained easily in practical applications in some frequency regions, such as plasma [23], superconductors [24], semiconductors [25] and metals [26]. Compared to the conventional dielectric PCs, the PCs containing the ENG materials display strong spatial dispersion, and zero-$\bar{n}$ PBGs can also be obtained [11] which are not dependent on the incident angle, lattices, and polarization of EM waves. Thus, the tunable PCs containing the ENG materials become a new research focus, which has been investigated extensively. Up to now, the most extensive works are reported on the applications realized in one-dimensional (1D) or 2D PCs, such as the omnidirectional mirrors [27], omnidirectional filter [28] and omnidirectional reflector [29]. However, the 1D and 2D PCs structure in theory may not be very well in accordance with the real applications. Thus, the 3D PCs structure may be closer to the actual situation. Compared to 1D and 2D cases, the reports on the 3D PCs containing the ENG materials are few. Although some works on the 3D metals [30–32] and plasma [33] PCs in theory and experiment can be found, the effects dielectric constant of ENG materials on the dispersive are not discussed, or the effective dielectric function of ENG material is looked as a constant but a frequency-depended medium. The relationships between the surface-plasmon modes and lattices for PCs are not studied in 3D case. From these reports [33], we can know that if 3D PCs containing the ENG materials with high symmetry, such as face-centered-cubic (fcc) lattices, simple-cubic (sc) lattices, and body-centered-cubic (bcc) lattices, the complete PBGs hardly can be achieved. To solve this problem, the anisotropic dielectric has to be introduced into 3D PCs. However, as mentioned in our previous work [33], the 3D PCs with diamond lattices can easily realize the complete PBGs without introducing the anisotropic dielectric. In those reports [34, 35], our research group also investigated the dispersive properties of stop band gaps (SBGs) in the Γ-X and Γ-L directions for 3D PCs with fcc and diamond lattices as the ENG materials introduced, respectively. From the results in those reports, if we want to obtain the tunable switching gaps, the dielectric constant of background must be large, and inserted spheres must be pure. Unfortunately, technological difficulties can be found in fabricating such

kind of high symmetry 3D PCs. In order to realize the tuning all-optical switching in 3D PCs with low background dielectric constant, we can use double-shell structures to construct 3D PCs as mentioned by Chan et al. [31] and Aryal et al. [36]. On the other hand, there is still great demand for the wavelength division multiplexer (WDM) for communication purposes [37]. Although introducing the Kerr nonlinear materials into PCs can realize WDM [38], the larger pump energy for nonlinear materials may become a barrier for realizing the integrated all-optical logic devices. As we know, the key point in realizing WDM is to obtain the tunable switching gaps [38]. In other words, if the switching state of PCs is changed, WDM can be realized. Thus, WDM can be realized easily by the 3D PCs containing ENG materials.

As mentioned above, the aims of this paper are to investigate the optical properties and switching state of 3D PCs with diamond lattices which are composed of the core isotropic dielectric spheres with surrounded by the ENG materials shells inserted in the air based on a modified plane wave expansion (PWE) method, and the unusual properties of surface-plasmon modes are also studied. A more general Drude-like model is used to describe the effective dielectric function of ENG material, and the damping factor also is considered. This paper is organized as follows. The equations computing the band structures are presented in Section 2. In Section 3, the influences of the radius of core dielectric sphere, relative dielectric constant of background, dielectric constant of ENG material and electronic plasma frequency on optical properties and switching state of such 3D PCs are investigated, respectively. The unusual properties of surface-plasmon modes can also be found in this section. Finally, conclusions are given in Section 4. An $e^{-j\omega t}$ time-dependence is implicit through the paper, with t the time, and $j = \sqrt{-1}$. We also consider c as light speed in vacuum.

2. THEORETICAL MODEL AND NUMERICAL METHOD

The first irreducible Brillouin zone and schematic structure of such 3D PCs containing the ENG materials with diamond lattices can be found in Figure 1. As shown in Figure 1, the high symmetry points have the coordinate as $\Gamma\,(0,\,0,\,0)$, $X = (2\pi/a,\,0,\,0)$, $W = (2\pi/a,\,\pi/a,\,0)$, $K = (1.5\pi/a,\,1.5\pi/a,\,0)$, $L = (\pi/a,\,\pi/a,\,\pi/a)$, and $U = (2\pi/a,\,0.5\pi/a,\,0.5\pi/a)$. The (1 0 0) and (1 1 1) directions can be described by the points L, Γ and X. Assuming dielectric background, the dielectric core and ENG materials are isotropic and homogeneous, and the relative dielectric functions are ε_b, ε_a and ε_p, respectively. As plotted in Figure 1(b), we consider the radius of the shells, radius of the core spheres and lattice constant as R_2, R_1 and a, respectively. In our numerical calculations, the ENG material is assumed frequency-dependent, and ε_p can be written as [34, 35]

$$\varepsilon_p(\omega) = \varepsilon_c - \frac{\omega_p^2}{\omega(\omega + j\gamma)} \tag{1}$$

where ε_c, ω_p and γ are the dielectric constant of ENG material, electronic plasma frequency and damping factor that contribute to the absorption and losses, respectively. In order to achieve the dispersive curves of PCs, many numerical methods can be used [39–41]. Among those methods, PWE method is the most popular one to obtain the band structures, although there are many shortcomings, such as convergence problem and large number of plane waves [42, 43]. Recently, the band structures for the PCs containing the Drude-type materials, such as plasma [44] and metal [45], can be computed successfully by a modified PWE method, which can compute the general nonlinear eigenvalue equation by a standard linearization technique. Thus, the PCs composed of the core spheres surrounded by the ENG material shells inserted in the air can be calculated easily by such a method. In this paper, the same technique will also be used to calculate the band structures of such 3D PCs. We consider the relative dielectric constant of core dielectric sphere to be 13.9, and the Maxwell's equation for the magnetic field in such 3D PCs can be expressed as:

$$\nabla \times \left[\frac{1}{\boldsymbol{\varepsilon}(\mathbf{r})}\nabla \times \mathbf{H}\right] = \frac{\omega^2}{c^2}\mathbf{H} \tag{2}$$

Since $\boldsymbol{\varepsilon}(\mathbf{r})$ is periodic, we can use Bloch's theorem to expand the $\mathbf{H}$ field in term of plane wave,

$$\mathbf{H}(\mathbf{r}) = \sum_{\mathbf{G}}\sum_{\lambda=1}^{2} h_{\mathbf{G},\lambda}\,\widehat{\mathbf{e}}_\lambda e^{[j(\mathbf{k}+\mathbf{G})\cdot\mathbf{r}]} \tag{3}$$

where $\mathbf{k}$ is a wave vector in the Brillouin zone of lattice, $\mathbf{G}$ a reciprocal-lattice vector, and $\widehat{\mathbf{e}}_{\mathbf{1}}$, $\widehat{\mathbf{e}}_2$ are orthogonal unit vectors that are both perpendicular to wave vector $\mathbf{k}+\mathbf{G}$ because of the transverse character of magnetic field $\mathbf{H}$ (i.e., $\nabla\cdot\mathbf{H}=0$). According to the modified PWE method [33–35], the dielectric constant dyadic can also be expanded in its Fourier form as

$$\varepsilon^{-1}(\mathrm{r})=\boldsymbol{\varepsilon}^{-1}_{\mathbf{G},\mathbf{G}'}=\sum_{\mathbf{G}}\kappa(\mathrm{G})\mathrm{e}^{\mathbf{jG}\cdot\mathbf{r}} \tag{4}$$

$$\kappa_{\mathbf{G},\mathbf{G}'}=\begin{cases}\left(\dfrac{\omega^2+j\gamma\omega}{\varepsilon_c\omega^2+j\varepsilon_c\gamma\omega-\omega_p^2}-\dfrac{1}{\varepsilon_b}\right)f_2+\left(\dfrac{1}{\varepsilon_a}-\dfrac{\omega^2+j\gamma\omega}{\varepsilon_c\omega^2+j\varepsilon_c\gamma\omega-\omega_p^2}\right)f_1+\dfrac{1}{\varepsilon_b}, & |\mathbf{G}-\mathbf{G}'|=0\\ \left(\dfrac{\omega^2+j\gamma\omega}{\varepsilon_c\omega^2+j\varepsilon_c\gamma\omega-\omega_p^2}-\dfrac{1}{\varepsilon_b}\right)\cdot 3f_2\left(\dfrac{\sin(|\mathbf{G}-\mathbf{G}'|R_2)-(|\mathbf{G}-\mathbf{G}'|R_2)\cos(|\mathbf{G}-\mathbf{G}'|R_2)}{(|\mathbf{G}-\mathbf{G}'|R_2)^3}\right)\cdot\cos\left(|\mathbf{G}-\mathbf{G}'|\cdot\mathbf{R_0}\right) & \\ +\left(\dfrac{1}{\varepsilon_a}-\dfrac{\omega^2+j\gamma\omega}{\varepsilon_c\omega^2+j\varepsilon_c\gamma\omega-\omega_p^2}\right)\cdot 3f_1\left(\dfrac{\sin(|\mathbf{G}-\mathbf{G}'|R_1)-(|\mathbf{G}-\mathbf{G}'|R_1)\cos(|\mathbf{G}-\mathbf{G}'|R_1)}{(|\mathbf{G}-\mathbf{G}'|R_1)^3}\right)\cdot\cos(|\mathbf{G}-\mathbf{G}'|\cdot\mathbf{R_0}), & |\mathbf{G}-\mathbf{G}'|\neq 0\end{cases} \tag{5}$$

where the vector $\mathbf{R_0}$ is $(0.125a,\ 0.125a,\ 0.125a)$, $f_1=(8\pi R_1^3)/(3V_m)$ the filling factor of the dielectric core spheres, and $f_2=(8\pi R_2^3)/(3V_m)$ the filling factor of the ENG-material-dielectric spheres, respectively. V_m is the volume of unit cell. Substituting Eq. (3) and Eq. (4) into Eq. (2), the following linear matrix equations can be obtained

$$\sum_{\mathbf{G}',\lambda'}H^{\lambda,\lambda'}_{\mathbf{G},G'}h_{\mathbf{G}',\lambda'}=\frac{\omega^2}{c^2}h_{\mathbf{G},\lambda} \tag{6}$$

where

$$H^{\lambda,\lambda'}_{\mathbf{G},\mathrm{G}'}=|\mathbf{k}+\mathrm{G}|\left|\mathbf{k}+\mathrm{G}'\right|\begin{pmatrix}\widehat{\mathbf{e}}_{\mathbf{2}}\cdot\boldsymbol{\varepsilon}^{-1}_{\mathbf{G},\mathrm{G}'}\cdot\widehat{\mathbf{e}}_{\mathbf{2}'} & -\widehat{\mathbf{e}}_{\mathbf{2}}\cdot\boldsymbol{\varepsilon}^{-1}_{\mathbf{G},\mathrm{G}'}\cdot\widehat{\mathbf{e}}_{\mathbf{1}'}\\ -\widehat{\mathbf{e}}_{\mathbf{1}}\cdot\boldsymbol{\varepsilon}^{-1}_{\mathbf{G},\mathrm{G}'}\cdot\widehat{\mathbf{e}}_{\mathbf{2}'} & \widehat{\mathbf{e}}_{\mathbf{1}}\cdot\boldsymbol{\varepsilon}^{-1}_{\mathbf{G},\mathrm{G}'}\cdot\widehat{\mathbf{e}}_{\mathbf{1}'}\end{pmatrix} \tag{7}$$

where $\boldsymbol{\varepsilon}^{-\mathbf{1}}_{\mathbf{G},\mathbf{G}'}=\kappa(\mathrm{G}-\mathbf{G}')$. We can write $h_{\mathbf{G},\lambda}$ of $\mathbf{H}(\mathrm{r})$ in the form [33–35]

$$h_{\mathbf{G},\lambda}=\sum_{\mathbf{G}}B(\mathbf{k}|\mathbf{G})e^{j(\mathbf{k}+\mathrm{G})\cdot\mathbf{r}} \tag{8}$$

We can obtain the equation for the coefficients $\{B(\mathbf{k}|\mathbf{G})\}$

$$\begin{aligned}&\left(\left(\frac{\omega^2+j\gamma\omega}{\varepsilon_c\omega^2+j\varepsilon_c\gamma\omega-\omega_p^2}-\frac{1}{\varepsilon_b}\right)f_2+\left(\frac{1}{\varepsilon_a}-\frac{\omega^2+j\gamma\omega}{\varepsilon_c\omega^2+j\varepsilon_c\gamma\omega-\omega_p^2}\right)f_1+\frac{1}{\varepsilon_b}\right)\cdot|\mathbf{k}+\mathbf{G}|\left|\mathbf{k}+\mathrm{G}'\right|\cdot\overleftrightarrow{\mathbf{F}}\cdot B\left(\mathbf{k}|\mathbf{G}\right)\\ &+\sum_{\mathbf{G}'_{\parallel}}{}'\left(\left(\left(\frac{\omega^2+j\gamma\omega}{\varepsilon_c\omega^2+j\varepsilon_c\gamma\omega-\omega_p^2}-\frac{1}{\varepsilon_b}\right)\cdot 3f_2\left(\frac{\sin(|\mathbf{G}-\mathbf{G}'|R_2)-(|\mathbf{G}-\mathbf{G}'|R_2)\cos\left(|\mathbf{G}-\mathbf{G}'|R_2\right)}{(|\mathbf{G}-\mathbf{G}'|R_2)^3}\right)\right.\right.\\ &\left.\left.+\left(\frac{1}{\varepsilon_a}-\frac{\omega^2+j\gamma\omega}{\varepsilon_c\omega^2+j\varepsilon_c\gamma\omega-\omega_p^2}\right)3f_1\left(\frac{\sin(|\mathbf{G}-\mathbf{G}'|R_1)-(|\mathbf{G}-\mathbf{G}'|R_1)\cos(|\mathbf{G}-\mathbf{G}'|R_1)}{(|\mathbf{G}-\mathbf{G}'|R_1)^3}\right)\right)\right.\\ &\left.\cdot\cos\left(|\mathbf{G}-\mathbf{G}'|\cdot\mathbf{R_0}\right)\right)\cdot|\mathbf{k}+\mathrm{G}|\left|\mathbf{k}+\mathrm{G}'\right|\cdot\overleftrightarrow{\mathbf{F}}\cdot B\left(\mathbf{k}|\mathbf{G}'\right)=\frac{\omega^2}{c^2}B(\mathbf{k}|\mathbf{G})\end{aligned} \tag{9}$$

where the prime on the sum over $\mathbf{G}'$ indicates that the term with $\mathbf{G}'=\mathbf{G}$ is omitted. We consider $\overleftrightarrow{\mathbf{F}}=\begin{pmatrix}\widehat{\mathbf{e}}_{\mathbf{2}}\cdot\widehat{\mathbf{e}}_{\mathbf{2}'} & -\widehat{\mathbf{e}}_{\mathbf{2}}\cdot\widehat{\mathbf{e}}_{\mathbf{1}'}\\ -\widehat{\mathbf{e}}_{\mathbf{1}}\cdot\widehat{\mathbf{e}}_{\mathbf{2}'} & \widehat{\mathbf{e}}_{\mathbf{1}}\cdot\widehat{\mathbf{e}}_{\mathbf{1}'}\end{pmatrix}$. At this point we use the definition of a complex variable μ given by

$$\mu=\omega/c \tag{10}$$

the linear equation can be written as

$$\mu^4\overleftrightarrow{\mathbf{I}}-\mu^3\overleftrightarrow{\mathbf{I}}-\mu^2\overleftrightarrow{\mathbf{U}}-\mu\overleftrightarrow{\mathbf{V}}-\overleftrightarrow{\mathbf{W}}=0 \tag{11}$$

$$\overleftrightarrow{\mathbf{T}}(\mathbf{G}|\mathbf{G}') = -j\frac{\gamma}{c}\boldsymbol{\delta}_{\mathbf{G}\cdot\mathbf{G}'}, \tag{12a}$$

$$\begin{aligned}\overleftrightarrow{\mathbf{U}}(\mathbf{G}|\mathbf{G}') = &\left\{\frac{\omega_p^2}{\varepsilon_c c^2} + \left[\frac{1}{\varepsilon_b} + \left(\frac{1}{\varepsilon_c} - \frac{1}{\varepsilon_b}\right) f_2 + \left(\frac{1}{\varepsilon_a} - \frac{1}{\varepsilon_c}\right) f_1\right] \cdot \overleftrightarrow{\mathbf{M}}\right\} \boldsymbol{\delta}_{\mathbf{G}\cdot\mathbf{G}'} \\ &+ \left\{\left(\frac{1}{\varepsilon_c} - \frac{1}{\varepsilon_b}\right) 3f_2 \left(\frac{\sin(|\mathbf{G}-\mathbf{G}'|R_2) - (|\mathbf{G}-\mathbf{G}'|R_2)\cos(|\mathbf{G}-\mathbf{G}'|R_2)}{(|\mathbf{G}-\mathbf{G}'|R_2)^3}\right)\right. \\ &\left. + \left(\frac{1}{\varepsilon_a} - \frac{1}{\varepsilon_c}\right) 3f_1 \left(\frac{\sin(|\mathbf{G}-\mathbf{G}'|R_1) - (|\mathbf{G}-\mathbf{G}'|R_1)\cos\left(|\mathbf{G}-\mathbf{G}'|R_1\right)}{(|\mathbf{G}-\mathbf{G}'|R_1)^3}\right)\right\} \cdot \overleftrightarrow{\mathbf{M}}\end{aligned} \tag{12b}$$

$$\begin{aligned}\overleftrightarrow{\mathbf{V}}(\mathbf{G}|\mathbf{G}') = &\left\{j\frac{\gamma}{c}\left[\frac{1}{\varepsilon_b} + \left(\frac{1}{\varepsilon_c} - \frac{1}{\varepsilon_b}\right) f_2 + \left(\frac{1}{\varepsilon_a} - \frac{1}{\varepsilon_c}\right) f_1\right] \cdot \overleftrightarrow{\mathbf{M}}\right\} \boldsymbol{\delta}_{\mathbf{G}\cdot\mathbf{G}'} \\ &+ j\frac{\gamma}{c}\left(\left(\frac{1}{\varepsilon_c} - \frac{1}{\varepsilon_b}\right) 3f_2 \left(\frac{\sin\left(|\mathbf{G}-\mathbf{G}'|R_2\right) - \left(|\mathbf{G}-\mathbf{G}'|R_2\right)\cos\left(|\mathbf{G}-\mathbf{G}'|R_2\right)}{(|\mathbf{G}-\mathbf{G}'|R_2)^3}\right)\right. \\ &\left. + \left(\frac{1}{\varepsilon_a} - \frac{1}{\varepsilon_c}\right) 3f_1 \left(\frac{\sin(|\mathbf{G}-\mathbf{G}'|R_1) - (|\mathbf{G}-\mathbf{G}'|R_1)\cos\left(|\mathbf{G}-\mathbf{G}'|R_1\right)}{(|\mathbf{G}-\mathbf{G}'|R_1)^3}\right)\right) \cdot \overleftrightarrow{\mathbf{M}}\end{aligned} \tag{12c}$$

$$\begin{aligned}\overleftrightarrow{\mathbf{W}}(\mathbf{G}|\mathbf{G}') = &\left\{\left(-\frac{\omega_p^2}{\varepsilon_c\varepsilon_b c^2} - \frac{\omega_p^2}{\varepsilon_c\varepsilon_a c^2} f_1 + \frac{\omega_p^2}{\varepsilon_c\varepsilon_a c^2} f_2\right) \cdot \overleftrightarrow{\mathbf{M}}\right\} \delta_{\mathbf{G}\cdot\mathbf{G}'} \\ &+ \left(-\frac{\omega_p^2}{\varepsilon_c\varepsilon_a c^2} 3f_1 \left(\frac{\sin(|\mathbf{G}-\mathbf{G}'|R_1) - (|\mathbf{G}-\mathbf{G}'|R_1)\cos(|\mathbf{G}-\mathbf{G}'|R_1)}{(|\mathbf{G}-\mathbf{G}'|R_1)^3}\right)\right. \\ &\left. + \frac{\omega_p^2}{\varepsilon_c\varepsilon_a c^2} 3f_2 \left(\frac{\sin(|\mathbf{G}-\mathbf{G}'|R_2) - \left(|\mathbf{G}-\mathbf{G}'|R_2\right)\cos\left(|\mathbf{G}-\mathbf{G}'|R_2\right)}{(|\mathbf{G}-\mathbf{G}'|R_2)^3}\right)\right) \cdot \overleftrightarrow{\mathbf{M}}\end{aligned} \tag{12d}$$

where $\overleftrightarrow{\mathbf{M}} = |\mathbf{k}+\mathbf{G}||\mathbf{k}+\mathbf{G}'| \cdot \overleftrightarrow{\mathbf{F}} \cdot \cos(\mathbf{G}\cdot\mathbf{R_0})$, and the element of the $N \times N$ matrices are $\overleftrightarrow{\mathbf{T}}$, $\overleftrightarrow{\mathbf{U}}$, $\overleftrightarrow{\mathbf{V}}$ and $\overleftrightarrow{\mathbf{W}}$. This polynomial form can be transformed into a linear problem in $4N$ dimension by $\overleftrightarrow{\mathbf{Q}}$ that fulfills

$$\overleftrightarrow{\mathbf{Q}} z = \mu z, \quad \overleftrightarrow{\mathbf{Q}} = \begin{bmatrix} \mathbf{0} & \overleftrightarrow{\mathbf{I}} & \mathbf{0} & \mathbf{0} \\ \mathbf{0} & \mathbf{0} & \overleftrightarrow{\mathbf{I}} & \mathbf{0} \\ \mathbf{0} & \mathbf{0} & \mathbf{0} & \overleftrightarrow{\mathbf{I}} \\ \overleftrightarrow{\mathbf{W}} & \overleftrightarrow{\mathbf{V}} & \overleftrightarrow{\mathbf{U}} & \overleftrightarrow{\mathbf{T}} \end{bmatrix} \tag{13}$$

The complete solution of Eq. (11) is obtained by computing for the eigenvalues of Eq. (13). Of course, the real part of such eigenvalues can determine the dispersion relation.

3. RESULTS AND DISCUSSION

In order to investigate the optical properties and switching state of such 3D PCs, we consider a simpler case. We make ENG materials surround the dielectric sphere ($\varepsilon_a = 13.9$) as a shell structure. Such double-shell structures are inserted into the air ($\varepsilon_b = 1$). Without loss of generality, we use $\omega a/2\pi c$ to normalize the frequency region. We use a variable $\omega_{p0} = 2\pi c/a$ to define the electronic plasma frequency as $\omega_p = \omega_{pl} = 0.15\omega_{p0}$, and choose the damping factor as $\gamma = 0.02\omega_{pl}$, $\mu_a = 1$, $\mu_b = 1$, and $\mu_p = 1$, respectively. As mentioned above, ω_{p0} and ω_{pl} are the symbols to define the constants and have no any physical meanings. In our calculation, we use 729 plane waves to make the convergence accuracy better than 1% for the lower bands [46].

In order to calculate the PBGs for such 3D PCs, we developed a code based on the PWE method. We checked our results against band structures calculated by the finite-difference frequency-domain (FDFD) method [47]. The test case is the band structure of dielectric spheres arranged in the fcc structure with filling factor $f = 0.3$ and $\varepsilon_a = 12.96$, embedded in the ENG materials with $\omega_p = 0.3\pi c/a$ and $\gamma = 0.02\omega_p$. In Figure 1, the band structures calculated by the FDFD and PWE methods are displayed with different ω_p and γ. The black solid curves are the results obtained by the PWE method, and the red open circles are the results calculated by the FDFD method. As shown in Figure 1, excellent agreement can be observed between the two methods, and Figure 1(a) is in excellent agreement with Figure 2(d) in [46].

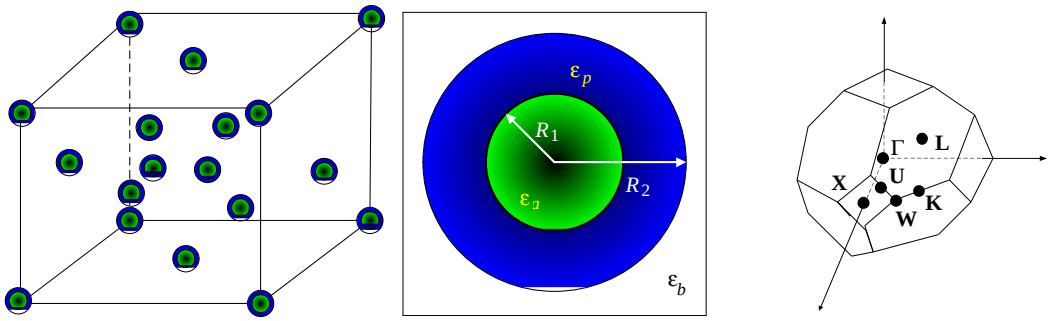

Figure 1. (a) Schematic structure of such 3D PCs. (b) Illustration of a unit cell of such 3D PCs. (c) The first irreducible Brillouin zone showing symmetry point used for obtaining the PBG.

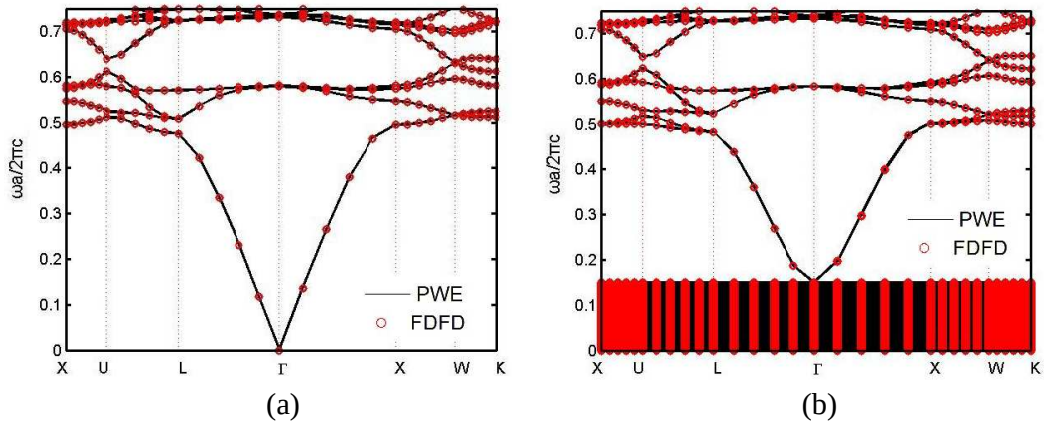

Figure 2. Dispersion curves for 3D fcc PCs with dielectric filling factor $f = 0.3$ and $\varepsilon_a = 12.96$ but with different ω_p and γ. (a) $\omega_p = 0$, $\gamma = 0$ and (b) $\omega_p = 0.15\omega_{p0}$, $\gamma = 0.02\omega_p$.

3.1. The Optical Properties and Switching State of Such 3D PCs

In Figure 3, we present the band structures for such 3D PCs with $\varepsilon_a = 13.9$, $\varepsilon_b = 1$, $\varepsilon_c = 1$, $R_1 = 0.1165a$ and $R_2 = 0.2165a$ but with different ω_p and γ. The red regions indicate the PBGs. As shown in Figure 3(a), if $\omega_p = 0$ and $\gamma = 0$, the ENG material shells can be looked as the air, and the two complete PBGs can be found in frequency region 0–$3.2\pi c/a$. The PBGs present themselves in 1.1416–1.1558 ($2\pi c/a$) and 1.3966–1.4489 ($2\pi c/a$), respectively. In this case, all optical switching can be realized. As shown in Figure 3(b), if $\omega_p = 0.15\omega_{p0}$ and $\gamma = 0.02\omega_{pl}$, not only such 3D PCs with double-shell structures containing the ENG material shells can produce the complete PBGs, but also one flatband region can be found at 1.1444–1.1592 ($2\pi c/a$), 1.399–1.4512 ($2\pi c/a$) and 0.0246–0.15

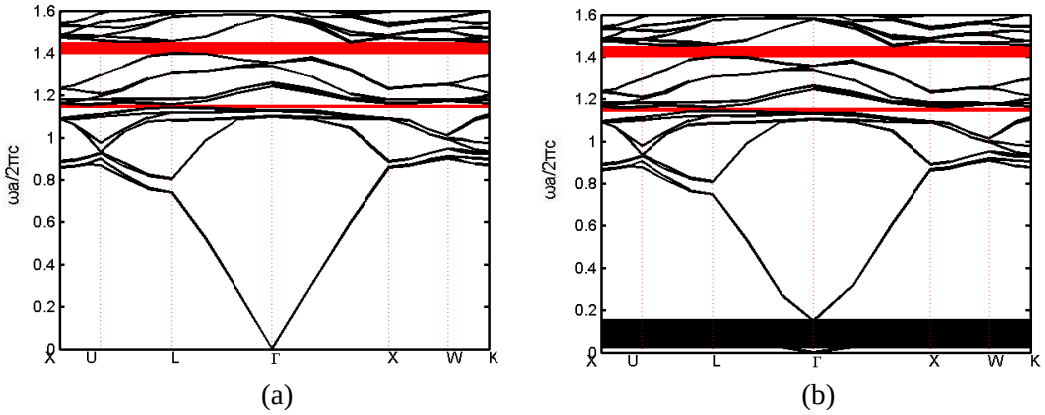

Figure 3. The band structures for such 3D PCs with $\varepsilon_a = 13.9$, $\varepsilon_b = 1$, $\varepsilon_c = 1$, $R_1 = 0.1165a$ and $R_2 = 0.2165a$ but with different ω_p and γ. (a) $\omega_p = 0$, $\gamma = 0$ and (b) $\omega_p = 0.15\omega_{p0}$, $\gamma = 0.02\omega_{pl}$, respectively. The red shaded region indicates PBGs.

$(2\pi c/a)$, respectively. Compared to the results in Figure 3(a), the edges of PBGs will shift upward to higher frequencies, and bandwidth of the first PBG can be enlarged, obviously. Thus, such double-shell structures can enhance the PBG as the ENG material shell is introduced. In other words, the switching state of such 3D PCs can be tuned by introducing the ENG materials. The SBGs in the (1 0 0) and (1 1 1) directions at X and L points are located in 0.7427–0.8108 $(2\pi c/a)$ and 0.8689–0.8912 $(2\pi c/a)$, respectively. As mentioned in our previous works [34, 35], the complete PBGs and SBGs can be tuned by the parameters of the ENG materials. It means that the switching state can also be manipulated. As mentioned above, the optical switching can be realized in such PCs in which the dielectric core spheres are surrounded by the ENG materials shells in the air. The switching gaps can be obtained with on and off states in the different frequency regions. Thus, the WDM can be realized by the properties of switching state for such 3D PCs. In this paper, we only focus on the switching state and dispersive properties of the first two PBGs and first SBGs in (1 0 0) and (1 1 1) directions at X and L points for such 3D PCs containing the ENG materials shells in the frequency domain 0–$3.2\pi c/a$.

3.2. The Unusual Properties of Surface-Plasmon Modes

As we know [34, 35], if the ENG material is introduced into the 3D PCs, the multiflatbands can be found in the flatband region in the case of $\omega < \omega_p$. The existing multiflatbands can be explained by the existence of surface-plasmon modes [34, 35]. In the frequency region $\omega < \omega_p$, the real part of dielectric function of ENG material is negative, but that for background is positive. Thus, the dielectric will change sign at interface across the ENG materials shells and background. The plasmon modes will be observed. In order to study the surface-plasmon modes for such 3D PCs, we plot the band structures for such 3D PCs with $\varepsilon_a = 13.9$, $\varepsilon_b = 1$, $\varepsilon_c = 1$, $\omega_p = 0.15\omega_{p0}$, $\gamma = 0.02\omega_{pl}$ and $R_2 = 0.2165a$ but with the different R_1 in Figure 4. As shown in Figures 4(a)–(c), the band structures of such PCs are hardly changed. There exists a threshold value for the thickness of ENG material shell (R_2-R_1) to make R_1 have no effect on the band structures. It means that such double-shell structures can be equivalent to the pure ENG material spheres. This can make fabrication of pure ENG material spheres structure easily and save the material in the realization. In Figure 5, we present the dispersive curves for such 3D PCs with $R_1 = 0.03a$, $\varepsilon_b = 1$, $\varepsilon_c = 1$, $\omega_p = 0.15\omega_{p0}$, $\gamma = 0.02\omega_{pl}$ and $R_2 = 0.2165a$ but with different dielectrics of inserted core spheres. As shown in Figures 5(a)–(c), if $R_1 = 0.03a$, the band structures will be similar to each other as Te ($n_o = 4.8$, $n_e = 6.2$) [33, 46], $\varepsilon_a = 12.4$ and $\varepsilon_a = 13.9$ are considered, respectively. It also means that the critical value of the ENG materials shell can make ε_a have no effect on the dispersive properties. In Figure 6, we display the band structures for such PCs with a similar case to Figure 5 except for $\varepsilon_b = 20$ and inserted different dielectric core spheres. As shown in Figures 6(a)–(c), if $R_1 = 0.03a$, the band structures will be similar to each other. The complete PBGs can be observed, which present themselves at 0.2768–0.2877 $(2\pi c/a)$, 0.2768–0.2877

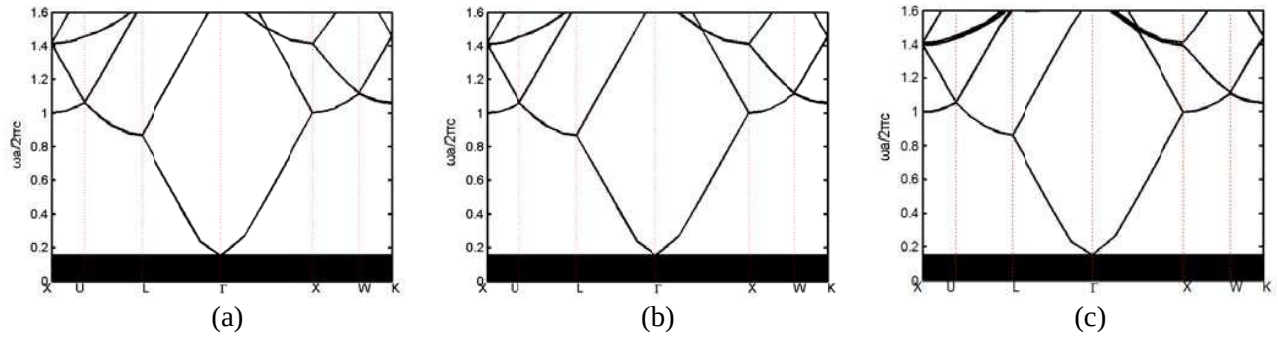

Figure 4. The band structures for such 3D PCs with $\varepsilon_a = 13.9$, $\varepsilon_b = 1$, $\varepsilon_c = 1$, $\omega_p = 0.15\omega_{p0}$, $\gamma = 0.02\omega_{pl}$ and $R_2 = 0.2165a$ but with the different radius of the core sphere. (a)$R_1 = 0$, (b) $R_1 = 0.02a$, and (c) $R_1 = 0.04a$, respectively.

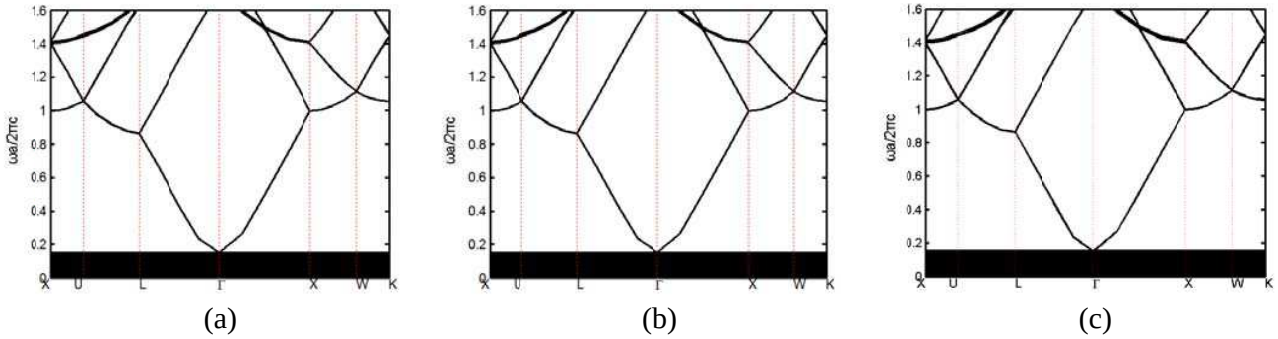

Figure 5. The band structures for such 3D PCs with $R_1 = 0.03a$, $\varepsilon_b = 1$, $\varepsilon_c = 1$, $\omega_p = 0.15\omega_{p0}$, $\gamma = 0.02\omega_{pl}$ and $R_2 = 0.2165a$ but with the different dielectric of inserted core spheres. (a) $\varepsilon_a = 12.4$, (b) $\varepsilon_a = 13.9$, and (c) Te ($n_o = 4.8$, $n_e = 6.2$), respectively.

($2\pi c/a$) and 0.2776–0.2882 ($2\pi c/a$). From the results in Figure 6, we can also know that the PBGs are hardly depended on ε_a as the thickness of ENG material shell is large enough. It needs to be noticed that the flatband region has also never changed. According to the results in the Figures 4–6, the unusual surface-plasmon modes can be achieved, which will not be affected by the radius and dielectric constant of the inserted core spheres as the thickness of ENG material shell is larger than a threshold value. The reason can be explained as that if the thickness of ENG material shell is large enough, and EM wave will be reflected by the coating shell since it cannot propagate through the ENG material shell, and the switching state of such PCs will not be changed.

In Figure 7, we present the band structures for such 3D PCs with $R_1 = 0.1165a$, $\varepsilon_a = 13.9$, $\varepsilon_b = 1$, $\varepsilon_c = 1$, $\omega_p = 0.15\omega_{p0}$, $\gamma = 0.02\omega_{pl}$ and $R_2 = 0.2165a$ but with the different lattices. As shown in Figures 7(a)–(c), the flatband regions can be observed as PCs with fcc, bcc and sc lattices. The flatband regions for such three lattices are 0.1187–0.15 ($2\pi c/a$), 0.1191–0.15 ($2\pi c/a$) and 0.1197–0.15 ($2\pi c/a$), respectively. From the results in Figure 7, we know that the unusual surface-plasmon modes can be found in the flatband region, and the upper edge of the flatband region will not depend on the topology of lattice. However, the lower edge of the flatband region will be different since the distance between the inserted core spheres is different. The results can be explained by the Maxwell-Garnett type effective medium theory. If the frequency of EM wave is less than ω_p, the effective dielectric ε_{eff} can be written as [48]

$$\varepsilon_{eff} = \frac{\varepsilon_b(1 + 2f_1\alpha_c)}{1 - f_1\alpha_c} \tag{14}$$

where $\alpha_c = \frac{\alpha_0+(R_1/R_2)^3\alpha_1(\varepsilon_b+2\varepsilon_p)/(\varepsilon_p+2\varepsilon_b)}{1+2(R_1/R_2)^3\alpha_1\alpha_0}$, $\alpha_1 = \frac{\varepsilon_a-\varepsilon_p}{\varepsilon_a+2\varepsilon_p}$, and $\alpha_0 = \frac{\varepsilon_p-\varepsilon_b}{\varepsilon_p+2\varepsilon_b}$. Moreover, $k = k_0\sqrt{\varepsilon_{eff}}$ and

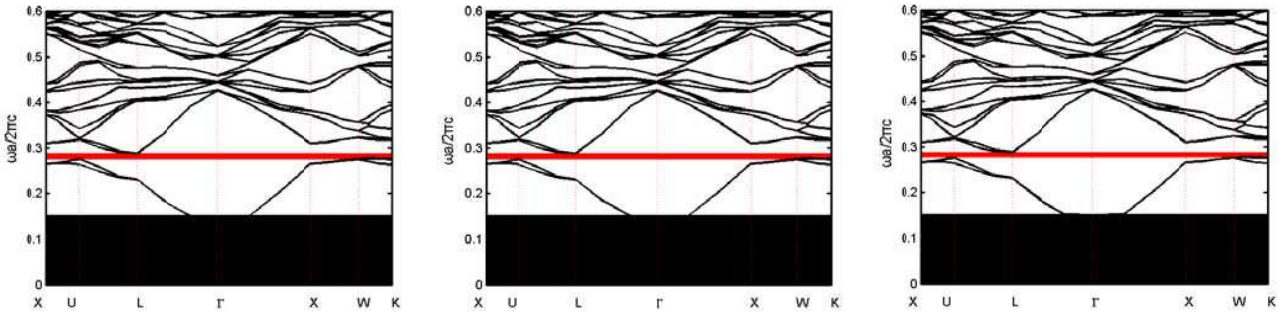

Figure 6. The band structures for such 3D PCs with $R_1 = 0.03a$, ε_b=20, $\varepsilon_c = 1$, $\omega_p = 0.15\omega_{p0}$, $\gamma = 0.02\omega_{pl}$ and $R_2 = 0.2165a$ but with the different dielectric of inserted core spheres. (a) $\varepsilon_a = 12.4$, (b) $\varepsilon_a = 13.9$, and (c) Te ($n_o = 4.8$, $n_e = 6.2$), respectively.

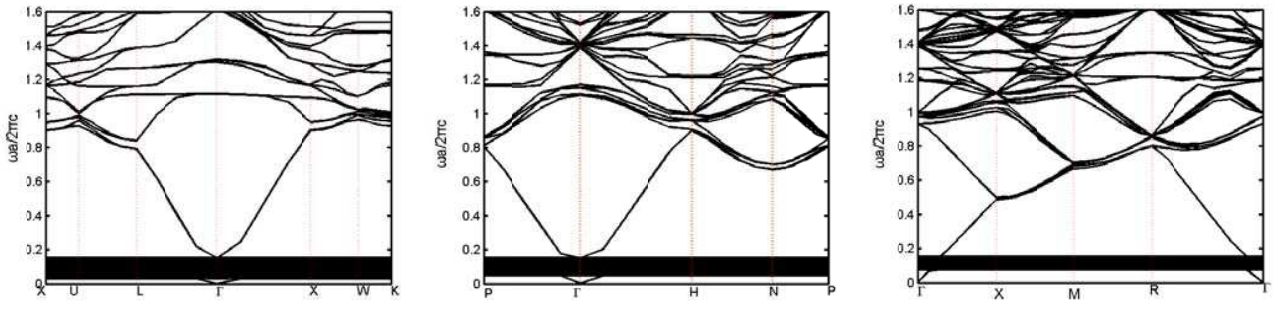

Figure 7. The band structures for such 3D PCs with $R_1 = 0.1165a$, $\varepsilon_a = 13.9$, $\varepsilon_b = 1$, $\varepsilon_c = 1$, $\omega_p = 0.15\omega_{p0}$, $\gamma = 0.02\omega_{pl}$ and $R_2 = 0.2165a$ but with the different lattices. (a) fcc lattices, (b) bcc lattices, and (c) sc lattices, respectively.

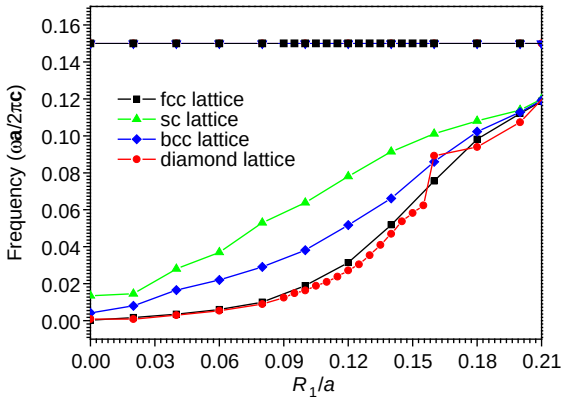

Figure 8. The upper and lower edges of flatband regions with $\varepsilon_a = 13.9$, $\varepsilon_b = 1$, $\varepsilon_c = 1$, $\omega_p = 0.15\omega_{p0}$, $\gamma = 0.02\omega_{pl}$ and $R_2 = 0.2165a$ as such PCs with the diamond, fcc, bcc and sc lattices as a function of R_1.

$k_0 = \omega/c$. Thus, we know that the dispersion relation will not depend on the topology of lattice since the wave vectors depends only on the dielectric constant of materials which are introduced into PCs, the filling of the core spheres and the thickness of ENG material shell. In order to further investigate the relationship between the PCs lattice and flatbands region, we plot both edges of flatband regions

with $\varepsilon_a = 13.9$, $\varepsilon_b = 1$, $\varepsilon_c = 1$, $\omega_p = 0.15\omega_{p0}$, $\gamma = 0.02\omega_{pl}$ and $R_2 = 0.2165a$ as the PCs with the diamond, fcc, bcc and sc lattices as a function of R_1 in Figure 8. As shown in Figure 8, the upper edges of flatband region for such three lattices will be never changed with increasing R_1, which are 0.15 $(2\pi c/a)$. It means that whether the core spheres existing or not will not influence the location of the upper edges frequencies. However, the lower edges of the flatband regions will shift upward to higher frequencies. If $R_1/a \leqq 0.04$, the lower edge frequencies of the flatband regions for such three lattices are near zero. As the value of R_1/a is increased from 0.04 to 0.21, the lower edge frequency for sc lattice has a larger value than the other three lattices. If $R_1/a = 0.21$, the lower edge frequencies of flatbands regions for such four lattices will be close to 0.119 $(2\pi c/a)$. On the other hand, it can also be shown from Figure 8 that the threshold value for R_1/a is $0.04a$, which can make the double-shell structure of such PCs look like a pure ENG material spheres inserted structure.

3.3. The Properties of Tunable Switching Gaps and SBGs

In Figure 9, we plot the dependences of the properties of the first two PBGs on R_1 with $\varepsilon_a = 13.9$, $\varepsilon_c = 1$, $\varepsilon_b = 1$, $\omega_p = 0.15\omega_{p0}$, $\gamma = 0.02\omega_{pl}$ and $R_2 = 0.2165a$, respectively. The shaded regions indicate the PBGs. Figure 9(a) illustrates that R_1 is an important parameter to the properties of switching. With increasing the value of R_1/a, both edges of the 1st and 2nd PBGs will shift to lower frequencies, and their bandwidths will first increase and then decrease. The maximum bandwidths of such two PBGs are

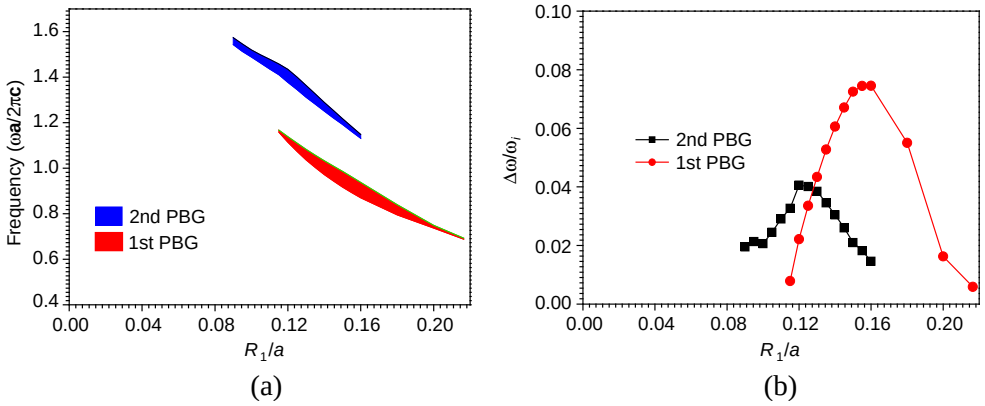

Figure 9. The effects of R_1 on first two PBGs and relative bandwidths for such 3D PCs with $\varepsilon_a = 13.9$, $\varepsilon_c = 1$, $\varepsilon_b = 1$, $\omega_p = 0.15\omega_{p0}$, $\gamma = 0.02\omega_{pl}$ and $R_2 = 0.2165a$, respectively. The shaded regions indicate the PBGs. (a) The PBGs and (b) the relative bandwidths, respectively.

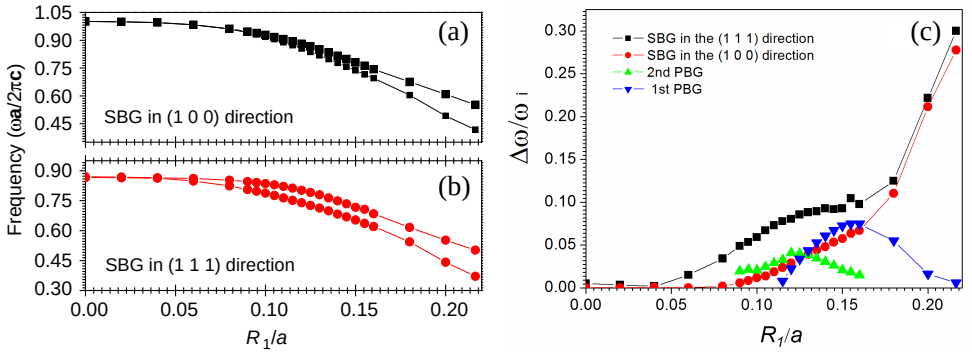

Figure 10. The effects of R_1 on 1st SBGs in the (1 0 0) and (1 1 1) directions at X and L points and relative bandwidths for such 3D PCs with $\varepsilon_a = 13.9$, $\varepsilon_c = 1$, $\varepsilon_b = 1$, $\omega_p = 0.15\omega_{p0}$, $\gamma = 0.02\omega_{pl}$ and $R_2 = 0.2165a$, respectively. (a) The SBG in the (1 0 0) direction at X point, (b) the SBG in the (1 1 1) direction at L point, and (c) the relative bandwidths for SBGs and PBG, respectively.

0.0691 and 0.0571 ($2\pi c/a$), which can be found in the cases of $R_1/a = 0.155$ and 0.12. If $R_1/a < 0.09$ and $R_1/a > 0.16$, the 2nd PBG will disappear. If $R_1/a < 0.115$, the 1st PBG cannot be observed. It means that the switching of such 3D PCs will turn from off to on state. The relative bandwidths ($\Delta\omega/\Delta\omega_i$) [34, 35] for such two PBGs are plotted in Figure 9(b). As shown in Figure 9(b), the relative bandwidths will first increase and then decrease. The maximum values of relative bandwidths are 0.0746 and 0.0406, which appear in the cases of $R_1/a = 0.16$ and 0.12, respectively. If $R_1/a < 0.9$, the relative bandwidth will equal zero, and the switching state is on. However, if $0.09 \leqslant R_1/a \leqslant 0.2165$, the off state can be obtained for such 3D PCs. In Figure 10, we plot the effects of R_1 on the 1st SBGs above the flatband region in the (1 0 0) and (1 1 1) directions at X and L points and their relative bandwidths for such 3D PCs with $\varepsilon_a = 13.9$, $\varepsilon_c = 1$, $\varepsilon_b = 1$, $\omega_p = 0.15\omega_{p0}$, $\gamma = 0.02\omega_{pl}$ and $R_2 = 0.2165a$, respectively. As shown in Figures 10(a)–(b), both edges of SBGs in (1 0 0) and (1 1 1) directions are downward to the lower frequency regions, and bandwidths of such two SBGs increase with increasing the value of R_1/a. Compared to the first two PBGs, the SBGs in (1 0 0) and (1 1 1) directions have larger bandwidths. The largest bandwidth can be found in the SBG in (1 0 0) direction. In Figure 10(c), the relative bandwidths for PBGs and SBGs are plotted. Figure 10(c) reveals that the relative bandwidths of SBGs increase with increasing R_1/a. The maximum relative bandwidths of SBGs in (1 0 0) and (1 1 1) directions are 0.2778 and 0.2999, which can be found in the case of R_1/a =0.2165, respectively. Compared to the maximum relative bandwidths of complete PBGs, the maximum relative bandwidths of SBGs in (1 0 0) and (1 1 1) directions are increased by 0.1474 and 0.1695, respectively. Figure 9(c) also show that the switching state of complete PBGs can be tuned by the radius of the dielectric core sphere, but the SBGs can not. In other words, the switching state of SBGs in (1 0 0) and (1 1 1) directions are always in off state. As mentioned above, the radius of the dielectric core sphere cannot affect the switching state of SBGs but can manipulate the switching state of complete PBGs.

In Figure 11, the dependences of the properties of PBGs on R_2 are plotted with $\varepsilon_a = 13.9$, $\varepsilon_c = 1$, $\varepsilon_b = 1$, $\omega_p = 0.15\omega_{p0}$, $\gamma = 0.02\omega_{pl}$ and $R_1 = 0.1165a$, respectively. As shown in Figure 11(a), the thicknesses of ENG materials shells have slight effect on the first two PBGs. With increasing R_2, the edges of PBG are upward to the higher frequencies, but the bandwidths will increase. As R_2/a is increased from 0.1265 to 0.2165, the bandwidths of the first two PBGs will be increased from 0.0123 to 0.0148 ($2\pi c/a$) and from 0.0518 to 0.0522 ($2\pi c/a$), respectively. The maximum bandwidths appear in the cases of $R_2 = 0.1865$ and $0.2165a$, respectively. As shown in Figure 11(a), the switching state cannot be manipulated only by changing R_2 as R_1 is certain, and the switching state is off. In Figure 11(b), the relative bandwidths are also plotted. Figure 11(b) shows that the relative bandwidths for the first two PBGs will increase with increasing R_2. We can find the minimum relative bandwidths at cases of $R_2 = 0.1265a$ and $0.1865a$, which are 0.0365 and 0.107, respectively. In Figure 12, we present the effects of R_2 on the 1st SBGs above the flatband region in (1 0 0) and (1 1 1) directions at X and L points and their relative bandwidths with $\varepsilon_a = 13.9$, $\varepsilon_c = 1$, $\varepsilon_b = 1$, $\omega_p = 0.15\omega_{p0}$, $\gamma = 0.02\omega_{pl}$ and $R_1 = 0.1165a$,

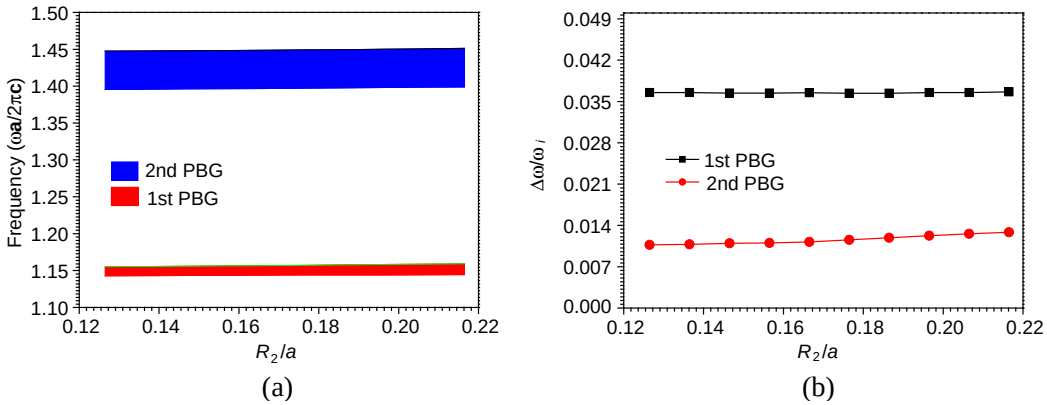

Figure 11. The effects of R_2 on first two PBGs and relative bandwidths for such 3D PCs with $\varepsilon_a = 13.9$, $\varepsilon_c = 1$, $\varepsilon_b = 1$, $\omega_p = 0.15\omega_{p0}$, γ=$0.02\omega_{pl}$ and $R_1 = 0.1165a$, respectively. The shaded regions indicate the PBGs. (a) The PBGs and (b) the relative bandwidths, respectively.

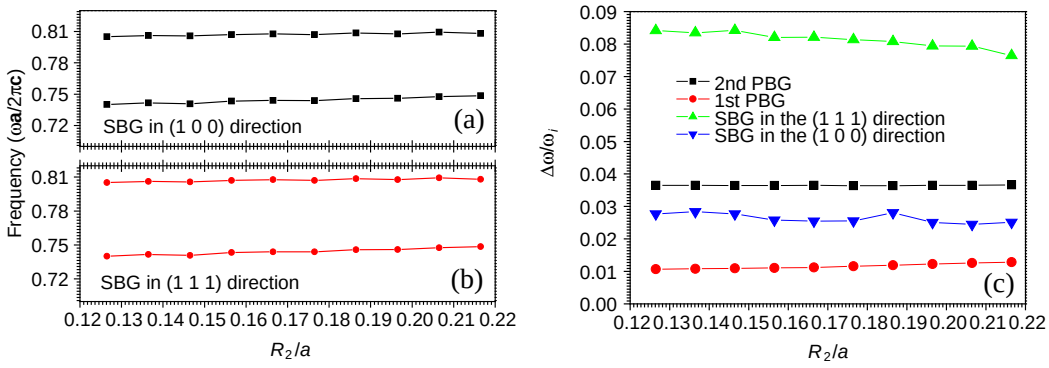

Figure 12. The effects of R_2 on 1st SBGs in the (1 0 0) and (1 1 1) directions at X and L points and relative bandwidths for such 3D PCs with $\varepsilon_a = 13.9$, $\varepsilon_c = 1$, $\varepsilon_b = 1$, $\omega_p = 0.15\omega_{p0}$, $\gamma = 0.02\omega_{pl}$ and $R_1 = 0.1165a$, respectively. (a) The SBG in the (1 0 0) direction at X point, (b) the SBG in the (1 1 1) direction at L point, and (c) the relative bandwidths for SBGs and PBG, respectively.

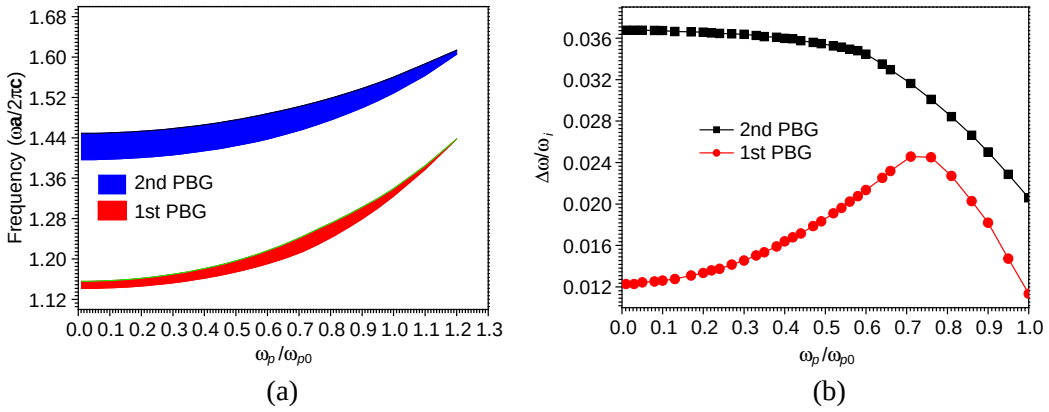

Figure 13. The effects of ω_p on first two PBGs and relative bandwidths for such 3D PCs with $R_2 = 0.2165a$, $\varepsilon_a = 13.9$, $\varepsilon_c = 1$, $\varepsilon_b = 1$, $\gamma = 0.02\omega_{pl}$ and $R_1 = 0.1165a$, respectively. The shaded regions indicate the PBGs. (a) The PBGs and (b) the relative bandwidths, respectively.

respectively. As shown in Figures 12(a)–(b), both edges and bandwidths of SBGs in (1 0 0) and (1 1 1) directions are increased with increasing R_2. Compared to the SBG in (1 0 0) direction, the SBG in (1 1 1) direction has a larger bandwidth. In Figure 12(c), the relative bandwidths for SBGs and PBGs are plotted. As shown in Figure 11(c), with increasing R_2, the relative bandwidths of SBG in (1 0 0) direction and the 2nd PBG are almost unchanged which are nearly 0.025 and 0.036, respectively. However, the relative bandwidths of SBG in (1 1 1) direction and the 1st PBG will decrease and increase as R_2 increased, and the maximum values are 0.0841 and 0.0129 for the cases of $R_1 = 0.1265a$ and $0.2165a$, respectively. Compared with the results in Figure 12, the maximum relative bandwidth can be found in the SBG in (1 1 1) direction. Consequently, if the value of R_1 is certain, the switching state cannot be changed by R_1.

In Figure 13, the effects of ω_p on the first two PBGs and relative bandwidths for such 3D PCs with $R_2 = 0.2165a$, $\varepsilon_a = 13.9$, $\varepsilon_c = 1$, $\varepsilon_b = 1$, $\gamma = 0.02\omega_{pl}$ and $R_1 = 0.1165a$ respectively, are plotted. As shown in Figure 13(a), the edges of the first PBGs will be upward to higher frequencies with increasing ω_p. For the 1st PBG, the bandwidth will first increase then decrease, but that for 2nd PBG will decease as ω_p increased. The switching state of PCs can be changed from off to on state. If $\omega_p/\omega_{p0} > 1.2$, both PBGs will disappear. The switching state becomes on. We also know that the maximum bandwidth for both PBGs can be observed in the cases of $\omega_p/\omega_{p0} = 0.71$ and 0.01, which are 0.0305 and 0.0523 $(2\pi c/a)$, respectively. It means that the switching state is easier to manipulate in high-ω_p region. It can also be

explained in physics that if ω_p is large enough, the effective permittivity can be less than 1. It means that the refractive contrast and average refractive index for such 3D PCs are changed. Thus, ω_p is an every important parameter to tune the switching state of PCs since the electronic plasma frequency of ENG materials can always be modulated by many external parameters such as the electric field, the external magnetic field and the temperature. The relative bandwidths are plotted in Figure 13(b). Figure 13(b) illustrates that the relative bandwidth for the 1st PBG will first increase then decrease, but that for 2nd PBG will decrease with increasing ω_p, and the maximum relative bandwidths are 0.0246 and 0.0368, which can be found in cases of 0.71 and 0.01. If $\omega_p/\omega_{p0} < 1.2$, the off state can be found. Compared the maximum relative bandwidths with the case of $\omega_p/\omega_{p0} = 0.17$, the relative bandwidths for the first two PBGs are increased by 0.0115 and 0.0001, respectively. In Figure 14, we plot the effects of ω_p on the 1st SBGs in (1 0 0) and (1 1 1) directions at X and L points and their relative bandwidths with $R_2 = 0.2165a$, $\varepsilon_a = 13.9$, $\varepsilon_c = 1$, $\varepsilon_b = 1$, $\gamma = 0.02\omega_{pl}$ and $R_1 = 0.1165a$, respectively. As shown in Figures 14(a)–(b), the edges of SBGs are upward to higher frequency regions, and bandwidths are increased first and then decreased with increasing ω_p. There is a jump point in band structures. The SBGs will be closed at the case of $\omega_p/\omega_{p0} = 0.64$ firstly, then a wider SBGs will appear in higher frequency. The bandwidths of SBG are larger than previous disappeared ones. This can also be explained in physics that increasing ω_p means that the space averaged dielectric constant of such 3D PCs becomes less and that the SBGs can be manipulated with changing PBGs [34, 35]. The SBG

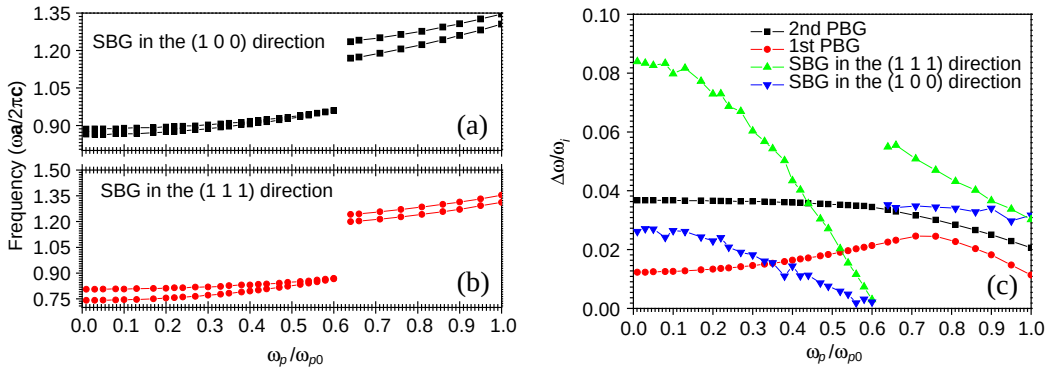

Figure 14. The effects of ω_p on 1st SBGs in the (1 0 0) and (1 1 1) directions at X and L points and relative bandwidths for such 3D PCs with $R_2 = 0.2165a$, $\varepsilon_a = 13.9$, $\varepsilon_c = 1$, $\varepsilon_b = 1$, $\gamma = 0.02\omega_{pl}$ and $R_1 = 0.1165a$, respectively. (a) The SBG in the (1 0 0) direction at X point, (b) the SBG in the (1 1 1) direction at L point, and (c) the relative bandwidths for SBGs and PBG, respectively.

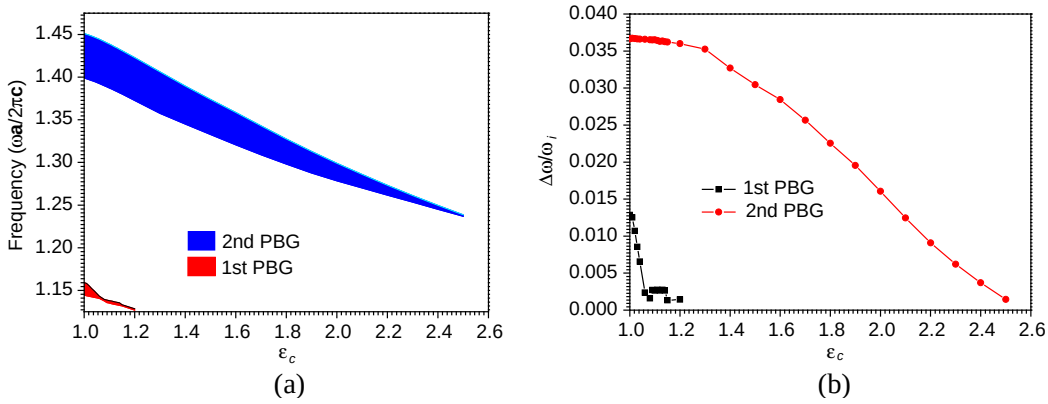

Figure 15. The effects of ε_c on first two PBGs and relative bandwidths for such 3D PCs with $R_2 = 0.2165a$, $\varepsilon_a = 13.9$, $\varepsilon_b = 1$, $\omega_p = 0.15\omega_{p0}$, $\gamma = 0.02\omega_{pl}$ and $R_1 = 0.1165a$, respectively. The shaded regions indicate the PBGs. (a) The PBG and (b) the relative bandwidth, respectively.

in (1 1 1) direction has a larger bandwidth than that in (1 0 0) direction. The maximum bandwidths for these two SBGs are 0.0649 and 0.066 ($2\pi c/a$) in the cases of $\omega_p/\omega_{p0} = 0.01$ and 0.6, respectively. The bandwidths of SBGs and PBGs are also presented in Figure 13(c). As shown in Figure 14(c), the larger relative bandwidths can be obtained in the SBG in (1 1 1) direction. The maximum bandwidths of these two SBGs and PBGs are 0.0839, 0.0555, 0.0246 and 0.0368, which can be observed in the cases of $\omega_p/\omega_{p0} = 0.01$, 0.64, 0.74 and 0.01, respectively. Compared to the case of $\omega_p/\omega_{p0} = 0.17$, the relative bandwidths of SBGs and PBGs are increased by 0.0066, 0.031, 0.0305 and 0.0523, respectively. It is noticed that there is a frequency region, which can make switching state of PCs change form off to on. It means that such 3D PCs can be applied in designing WDM [37]. It is also noticed that the damping factor of the ENG materials has no effect on switching state and SBGs since it only determines the degree of energy absorbed [34, 35]. As mentioned before, the switching properties of such 3D PCs can be tuned obviously by ω_p, and the on state can be obtained in the high-ω_p region.

In Figure 15, the effects of ε_c on the switching properties of the first two PBGs are plotted with $R_2 = 0.2165a$, $\varepsilon_a = 13.9$, $\varepsilon_b = 1$, $\omega_p = 0.15\omega_{p0}$, $\gamma = 0.02\omega_{pl}$ and $R_1 = 0.1165a$, respectively. Figure 15(a) shows that the edges of PBGs will shift to lower frequencies, and the bandwidths decease with increasing ε_c. If $\varepsilon_c > 1.2$, the 1st PBG will disappear, but the 2nd PBG will be closed at $\varepsilon_c = 2.5$. It means that the switching state of such PCs can also be tuned by ε_c. If $\varepsilon_c \leqq 1.2$, the switching state will be off, and the frequency region of 'off' state will be changed and moved to higher frequencies as $1.2 < \varepsilon_c \leqq 2.5$. The on state can be obtained as $\varepsilon_c > 2.5$. This can also be explained in physics that increasing ε_c means that the refractive contrast and average refractive index for such 3D PCs becomes larger and that the PBGs can be manipulated [49]. The maximum bandwidths of the first two PBGs are 0.0148 and 0.0523 ($2\pi c/a$), which can be observed in the cases of $\varepsilon_c = 1$. We plot the relative bandwidths in Figure 15(b). As shown in Figure 15(b), the relative bandwidths of the first two PBGs will decrease with increasing ε_c. The maximum bandwidths of the first two PBGs are 0.0129 and 0.0366, which can be observed in the cases of $\varepsilon_c = 1$, respectively. In Figure 16, we plot the effects of ε_c on the 1st SBGs in (1 0 0) and (1 1 1) directions at X and L points and their relative bandwidths with $R_2 = 0.2165a$, $\varepsilon_a = 13.9$, $\varepsilon_b = 1$, $\omega_p = 0.15\omega_{p0}$, $\gamma = 0.02\omega_{pl}$ and $R_1 = 0.1165a$, respectively. As shown in Figures 16(a)–(b), the edges of SBGs will shift downward to lower frequencies with increasing ε_c. For the 1st SBG in (1 0 0) direction, the bandwidth will increase, but that for the 1st SBG in (1 1 1) direction, the bandwidth will increase first then decrease. The maximum bandwidths of SBGs are 0.0896 and 0.201 ($2\pi c/a$), respectively. Compared to the SBG in (1 1 1) direction, the SBG in (1 0 0) direction has a larger bandwidth. The relative bandwidths of SBGs and PBGs are plotted in Figure 16(c). As shown in Figure 16(c), the SBG in (1 1 1) direction has larger relative bandwidth than those for PBGs and SBG in (1 0 0) direction. The maximum bandwidths of such two SBGs and first two PBGs are 0.2965, 0.3389, 0.0366 and 0.0129, which can be found in the cases of $\varepsilon_c = 2.5$, 2, 1 and 1, respectively. As mentioned above, the PBGs of such 3D PCs can be changed by ε_c, and the off state will appear in the low-ε_c region.

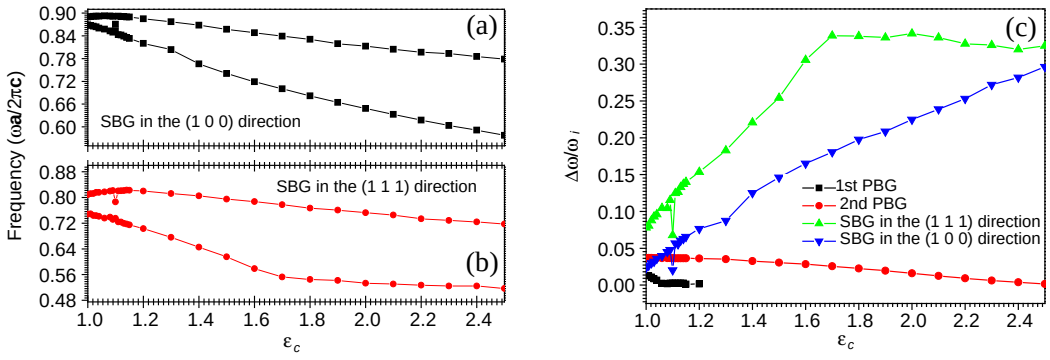

Figure 16. The effects of ε_c on 1st SBGs in the (1 0 0) and (1 1 1) directions at X and L points and relative bandwidths for such 3D PCs with $R_2 = 0.2165a$, $\varepsilon_a = 13.9$, $\varepsilon_b = 1$, $\omega_p = 0.15\omega_{p0}$, $\gamma = 0.02\omega_{pl}$ and $R_1 = 0.1165a$, respectively. (a) The SBG in the (1 0 0) direction at X point, (b) the SBG in the (1 1 1) direction at L point, and (c) the relative bandwidths for SBGs and PBG, respectively.

In Figure 17, the dependences of the properties of first two PBG on ε_b are plotted with $R_2 = 0.2165a$, $\varepsilon_a = 13.9$, $\varepsilon_c = 1$, $\omega_p = 0.15\omega_{p0}$, $\gamma = 0.02\omega_{pl}$ and $R_1 = 0.1165a$, respectively. As shown in Figure 17(a), the first two complete PBGs can be affected obviously by the background dielectric ε_b. With increasing ε_b, the edges and bandwidths of PBGs will be downward to lower frequencies. It is worth to notice that if $\varepsilon_b > 1.08$, the 1st PBG will disappear, and the 2nd PBG will be closed at $\varepsilon_b > 1.08$. The maximum bandwidths of the first two PBGs are 0.0148 and 0.0522 ($2\pi c/a$), which can be found in the cases of $\varepsilon_b = 1$. Figure 17(a) illustrates that the switching state of such 3D PCs can be changed by ε_b. If $\varepsilon_b \leqq 1.08$, the switching state is off. If $\varepsilon_b > 2.2$, the on state can be obtained, and the PBGs will disappear. In Figure 17(b), the curves of relative bandwidths can be found. As shown in Figure 17(b), the relative bandwidths of PBG will decrease with increasing ε_b. The maximum relative bandwidths are 0.0129 and 0.0366, which appear in the cases of $\varepsilon_b = 1$. Compared to the case of $\varepsilon_b = 2.2$, the relative bandwidths are decreased by 0.0129 and 0.0255. In Figure 18, we plot the effects of ε_b on the 1st SBGs in (1 0 0) and (1 1 1) directions at X and L points and their relative bandwidths with $R_2 = 0.2165a$, $\varepsilon_a = 13.9$, $\varepsilon_c = 1$, $\omega_p = 0.15\omega_{p0}$, $\gamma = 0.02\omega_{pl}$ and $R_1 = 0.1165a$, respectively. Figures 18(a)–(b) show that both edges of these two SBGs shift downward to lower frequencies with increasing ε_b. For SBG in (1 0 0) direction, the bandwidth is decreased as ε_b increases, but that for SBG in (1 0 0) direction first decreases and then increases, and a contraction point can be observed. The maximum bandwidths of these two SBGs are 0.0681 and 0.023 ($2\pi c/a$), which can be found in cases of $\varepsilon_b = 1$, respectively.

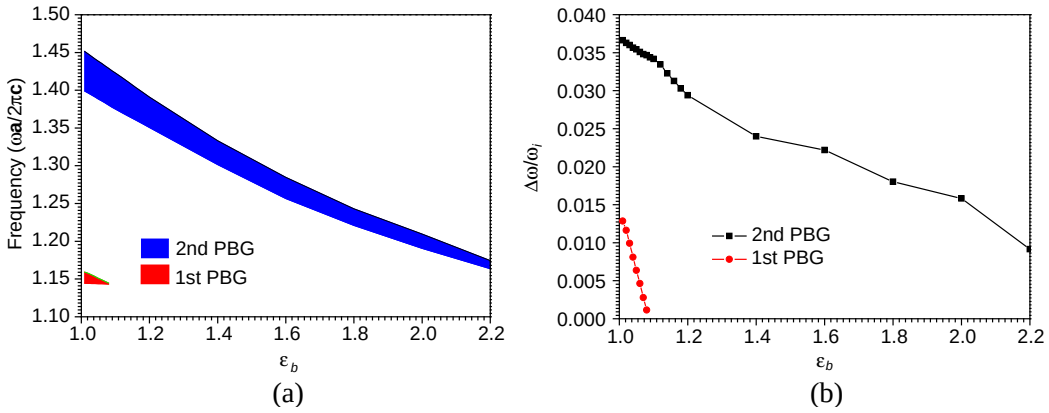

Figure 17. The effects of ε_b on first two PBGs and relative bandwidths for such 3D PCs with $R_2 = 0.2165a$, $\varepsilon_a = 13.9$, $\varepsilon_c = 1$, $\omega_p = 0.15\omega_{p0}$, $\gamma = 0.02\omega_{pl}$ and $R_1 = 0.1165a$, respectively. The shaded regions indicate the PBGs. (a) The PBGs, and (b) the relative bandwidths, respectively.

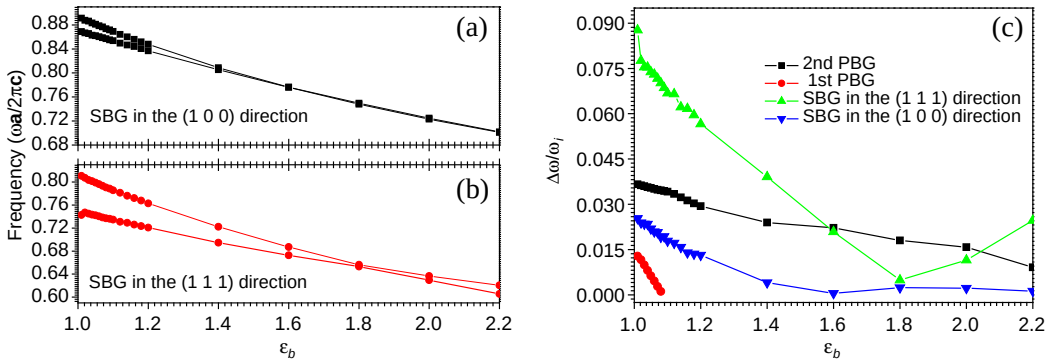

Figure 18. The effects of ε_b on 1st SBGs in the (1 0 0) and (1 1 1) directions at X and L points and relative bandwidths for such 3D PCs with $R_2 = 0.2165a$, $\varepsilon_a = 13.9$, $\varepsilon_c = 1$, $\omega_p = 0.15\omega_{p0}$, $\gamma = 0.02\omega_{pl}$ and $R_1 = 0.1165a$, respectively. (a) The SBG in the (1 0 0) direction at X point, (b) the SBG in the (1 1 1) direction at L point, and (c) the relative bandwidths for SBGs and PBG, respectively.

In Figure 18(c), the relative bandwidths for PBGs and SBGs are plotted. As shown in Figure 18(c), the relative bandwidths of the first two PBGs and SBG in (1 0 0) direction will decease, but that for SBG in (1 1 1) direction will decrease first then increase with increasing ε_b. The maximum relative bandwidths of PBGs and SBGs are 0.0129, 0.0366, 0.0253 and 0.0877, which appear in the cases of $\varepsilon_b = 1$, respectively. Compared to the case of $\varepsilon_b = 2.2$, the relative bandwidths of PBGs and these two SBGs are decreased by 0.024, 0.0631, 0.0129 and 0.0274, respectively. From the aforementioned discussions, the switching state of such 3D PCs can also be tuned obviously by ε_b. The off state can be obtained in low-ε_b region. This can be explained by that the refractive index contrasts of PCs are not large enough to open a PBG if ε_b is large enough [34, 35, 49]. On the other hand, the SBG in (1 0 0) direction will be closed in hight-ε_b region, but that in (1 1 1) direction will never disappear with increasing ε_b.

4. CONCLUSION

In summary, the PBG properties and switching state of 3D PCs with diamond lattices, which are composed of the core dielectric spheres with surrounded by the ENG materials shells inserted in the air, are theoretically studied in detail based on a modified PWE method. The equations for computing band structures for such 3D PCs are presented. Based on the numerical results, some conclusions can be drawn. Compared to the conventional inserted dielectric spheres structure, the complete PBG can be enlarged by the double-shell structure as the ENG materials are introduced. The optical switching state and SBGs in (1 0 0) and (1 1 1) directions can also be realized easily and modulated by the radius of core dielectric sphere, relative dielectric constant of background, dielectric constant of ENG material and electronic plasma frequency, respectively. It is worth to note that the switching state can be changed by ε_b, ε_c, ω_p and R_1, respectively. However, tuning γ and R_2 cannot tune the switching state of PCs as the radius of core dielectric sphere is certain. With increasing R_1, ε_c and ε_b, the edges of complete PBGs and SBGs will be downward to lower frequencies, and the larger relative bandwidth always can be found in SBG in the (1 1 1) direction. However, with increasing ω_p, the edges of first two PBGs and SBGs will shift upward to higher frequencies, the larger relative bandwidths of PBGs and SBGs can be found in low-ω_p region. The numerical simulations also show that the unusual surface-plasmon modes can be found in the flatband region. The unusual properties include the following points: firstly, there is a threshold value for the thickness of ENG materials shell, which can take the dispersive curves of such 3D double-shell structures PCs be similar to those obtained from the same structures containing the pure ENG materials spheres. In this case, the dielectric function of inserted core sphere will not affect the band structures. It means that we can achieve the PBGs by replacing the pure inserted sphere structures with such double-shell structures to make fabrication easily and save the material in the realization. Secondly, the upper edge of flatbands region does not depend on the topology of lattice, and the lower edge frequencies of flatbands regions for different lattices will tend to a constant as the ENG material shell is close to zero. As mentioned above, the presented 3D PCs with double-shell structures offer a novel way to realize the WDM.

ACKNOWLEDGMENT

This work was supported in part by the National Natural Science Foundation of China (Grant No. 61307052), in part by the Chinese Specialized Research Fund for the Doctoral Program of Higher Education (Grant No. 20123218110017), in part by the Jiangshu Province Science Foundation (Grant No. BK2011727), in part by the Fundamental Research Funds for the Central Universities (No. NZ2013302), and in part by the Foundation of Aeronautical Science (No. 20121852030).

REFERENCES

1. Yablonovitch, E., "Inhibited spontaneous emission of photons in solidstate physics and electronies," *Phys. Rev. Lett.*, Vol. 58, 2059–2061, 1987.
2. John, S., "Strong localization of photons in certain disordered dielectric superlattices," *Phys. Rev. Lett.*, Vol. 58, No. 23, 2486–2489, 1987.

3. Banerjee, A., "Enhanced refractometric optical sensing by using one-dimensional ternary photonic crystals," *Progress In Electromagnetics Research*, Vol. 89, 11–22, 2009.
4. Du, G. Q., H. T. Jiang, Z. S. Wang, and H. Chen, "Optical nonlinearity enhancement in heterostructures with thick metallic film and truncated photonic crystals," *Opt. Lett.*, Vol. 34, No. 5, 578580, 2009.
5. Liu, Q., Z. Ouyang, C. J. Wu, C. P. Liu, and J. C. Wang, "All-optical half adder based on cross structures in two-dimensional photonic crystals," *Opt. Exp.*, Vol. 16, No. 23, 18992–19000, 2008.
6. Zhang, H. F., M. Li, and S. B. Liu, "Defect mode properties of magnetized plasma photonic crystals," *Acta Phys. Sin.*, Vol. 58, No. 2, 1071–1076, 2009.
7. Zhang, H. F., S. B. Liu, X. K. Kong, B. R. Bian, and Y. Dai, "Omnidirectional photonic band gaps enlarged by Fibonacci quasi-periodic one-dimensional ternary superconductor photonic crystals," *Solid State Commun.*, Vol. 152, 2113–2119, 2012.
8. Fan, S. H., S. G. Johnson, J. D. Joannopoulos, C. Manolatou, and H. A. Haus, "Waveguide branches in photonic crystals," *J. Opt. Soc. Am. B*, Vol. 18, 162–165, 2001.
9. Kockaert, P., P. Tassin, I. Veretennicoff, G. V. der Sande, and M. Tlidi, "Beyond the zero-diffraction regime in optical cavities with a left-handed material," *J. Opt. Soc. Am. B*, Vol. 26, No. 12, B148–B155, 2009.
10. Wang, L., H. Chen, and S. Zhu, "Omnidirectional gap and defect mode of one-dimensional photonic crystals with single-negative materials," *Phys. Rev. B*, Vol. 70, 245102, 2004.
11. Chen, Y., "Broadband one-dimensional photonic crystals wave plate containing single-negative materials," *Opt. Exp.*, Vol. 18, No. 19, 19920–19929, 2010.
12. Veselago, V. G., "The electrodynamics of substance with simultaneously negative values of ε and μ," *Sov. Phys. Uspekhi*, Vol. 10, 509–514, 1968.
13. Smith, D. R., W. J. Padilla, D. C. Vier, S. C. Nemat-Nasser, and S. Schultz, "Composite medium with simultaneously negative permeability and permittivity," *Phys. Rev. Lett.*, Vol. 84, No. 18, 4184–4187, 2000.
14. Pendry, J. B., " Negative refraction makes a perfect len," *Phys. Rev. Lett.*, Vol. 85, No. 18, 3966–3969, 2000.
15. Morits, D. and C. R. Simovski, "Electromagnetic characterization of planar and bulk metamaterials: A theoretical study," *Phys. Rev. B*, Vol. 82, No. 16, 165114, 2010.
16. Smith, D. R., S. Schultz, P. Marko, and C. M. Soukoulis, "Determination of effective permittivity and permeability of metamaterials from reflection and transmission coefficients," *Phys. Rev. B*, Vol. 65, No. 19, 195104, 2002.
17. Liu X. and A. Alu, "Homogenization of quasi-isotropic metamaterials composed by dense arrays of magnetodielectric spheres," *Metamaterials*, Vol. 5, Nos. 2–3, 56–63, 2011.
18. Holloway, C. L., M. A. Mohamed, E. F. Kuester, and A. Dienstfrey, "Reflection and transmission properties of a metafilm: With an application to a controllable surface composed of resonant particles," *IEEE Trans. Electromagn. Compat.*, Vol. 47, No. 4, 853–865, 2005.
19. Kim, S., E. F. Kuester, C. L. Holloway, A. D. Scher, and J. Baker-Jarvis, "Boundary effects on the determination of metamaterial parameters from normal incidence reflection and transmission measurements," *IEEE Trans. Antennas Propag.*, Vol. 59, No. 6, 2226–2240, 2011.
20. Dimitriadis, A. I., D. L. Sounas, N. V. Kantartzis, C. Caloz, and T. D. Tsiboukis, "Surface susceptibility bianisotropic matrix model for periodic metasurfaces of uniaxially mono-anisotropic scatterers under oblique TE-wave incidence," *IEEE Trans. Antennas Propag.*, Vol. 60, No. 12, 5753–5767, 2012.
21. Penciu, R. S., K. Aydin, M. Kafesaki, T. Koschny, E. Ozbay, E. N. Economou, and C. M. Soukoulis, "Multi-gap individual and coupled split-ring resonator structures," *Opt. Exp.*, Vol. 16, No. 22, 18131–18144, 2008.
22. Sounas, D. L., N. V. Kantartzis, and T. D. Tsiboukis, "Focusing efficiency analysis and performance optimization of arbitrarily-sized DNG metamaterial slabs with losses," *IEEE Trans. Microwave Theory Techn.*, Vol. 54, No. 12, 4111–4121, 2006.

23. Zhang, H. F., S. B. Liu, X. K. Kong, L. Zou, C. Z. Li, and W. S. Qing, "Enhancement of omnidirectional photonic band gaps in one-dimensional dielectric plasma photonic crystals with a matching layer," *Physics Plasma*, Vol. 19, 022103, 2012.
24. Zhang, H. F., S. B. Liu, X. K. Kong, B. R. Bian, and X. Zhao, "Properties of omnidirectional photonic band gaps in Fibonacci quasi-periodic one-dimensional superconductor photonic crystals," *Progress In Electromagnetics Research B*, Vol. 40, 415–431, 2012.
25. Kamp, M., T. Happ, S. Mahnkopf, G. Duan, S. Anand, and A. Forchel, "Semiconductor photonic crystals for optoelectronics," *Phys. E*, Vol. 21, Nos. 2–4, 802–808, 2004.
26. Moroz, A., "Three-dimensional complete photonic-band-gap structure in the visible," *Phys. Rev. Lett.*, Vol. 83, No. 25, 5274–5277, 1999.
27. Krumbholz, N., K. Gerlach, F. Rutz, M. Koch, R. Piesiewicz, T. Kürner, and D. Mittleman, "Ominidirectional terahertz mirror: A key element for future terahertz communication systems," *Appl. Phys. Lett.*, Vol. 88, 202905, 2006.
28. Xu, K., X. Zheng, C. Li, and W. She, "Design of omnidirectional and multiple channeled filters using one-dimensional photonic crystals containing a defect layer with a negative refractive index," *Phys. Rev. E*, Vol. 71, No. 6, 066604, 2005.
29. Deng, X. H., J. T. Liu, J. H. Huang, L. Zou, and N. H. Liu, "Omnidirectional bandgaps in Fibonacci quasicrystal containing single-negative materials," *J. Phys.: Condens. Matt.*, Vol. 22, No. 5, 055403, 2010.
30. Wang, Z., C. T. Chan, W. Zhang, N. Ming, and P. Sheng, "Three-dimensional self-assembly of metal nanoparticles: Possible photonic crystal with a complete gap below the plasma frequency," *Phys. Rev. B*, Vol. 64, No. 11, 113108, 2001.
31. Chan, C. T., W. Y. Zhang, Z. L. Wang, X. Y. Lei, D. Zheng, W. Y. Tam, and P. Sheng, "Photonic band gaps from metallo-dielectric spheres," *Phys. B*, Vol. 279, Nos. 1–3, 150–154, 2000.
32. Zhang, W. Y., X. Y. Lei, Z. L. Wang, D. G. Zheng, W. Y. Tam, C. T. Chan, and P. Sheng, "Roubust photonic band gap from tunable scatterers," *Phys. Rev. Lett.*, Vol. 84, No. 13, 2853–2856, 2000.
33. Zhang, H. F., S. B. Liu, and X. K. Kong, "Properties of anisotropic photonic band gaps in three-dimensional plasma photonic crystals containing the uniaxial material with different lattices," *Progress In Electromagnetics Research*, Vol. 141, 267–289, 2013.
34. Zhang, H. F., S. B. Liu, and X. K. Kong, "Investigating the dispersive properties of the three-dimensional photonic crystals with face-centered-cubic lattices constaining epsilon-negative materials," *Appl. Phys. B*, Vol. 112, No. 4, 553–563, 2013.
35. Zhang, H. F., S. B. Liu, and X. K. Kong, "Study of the dispersive properties of three-dimensional photonic crystals with diamond lattices containing metamaterials," *Laser Phys.*, Vol. 23, No. 10, 105815, 2013.
36. Aryal, D. P., K. L. Tsakmakidis, and O. Hess, "Complete bandgap switching in photonic crystals," *Journal of New Physics*, Vol. 11, 073011, 2009.
37. Smajic, J., C. Hafner, and D. Erni, "Design and optimization of an achromatic photonic crystal bend," *Opt. Exp.*, Vol. 11, No. 12, 1378–1384, 2003.
38. Cicek, A. and B. Ulug, "Influnce of Kerr nonlinearity on the band structures of two-dimensional photonic crystals," *Optic Commun.*, Vol. 281, No. 14, 3924–3931, 2008
39. Jun, S., Y. S. Cho, and S. Im, "Moving least-square method for the band-structure calculation of 2D photonic crystals," *Opt. Exp.*, Vol. 11, No. 6, 541–551, 2003.
40. Chiang, P., C. Yu, and H. Chang, "Analysis of two-dimensional photonic crystals using a multidomain pseudospectral method," *Phys. Rev. E*, Vol. 75, No. 2, 026703, 2003.
41. Lou, M., Q. H. Liu, and Z. Li, "Spectral element method for band structures of three-dimensional anisotropic photonic crystals," *Phys. Rev. E*, Vol. 80, No. 5, 56702, 2012.
42. Sözüer, H. S., J. W. Haus, and R. Inguva, "Photonic bands: Convergence problems with the plane-wave method," *Phys. Rev. B*, Vol. 45, No. 24, 13962, 1992.
43. Li, L. and C. W. Haggans, "Convergence of the coupled-wave method for metallic lamellar diffraction gratings," *J. Opt. Soc. Am. A*, Vol. 10, 1184–1189, 1993.

44. Zhang, H. F., S. B. Liu, X. K. Kong, L. Zhou, C. Z. Li, and B. R. Bo, "Comment on 'photonic bands in two-dimensional microplasma array. I. Theoretical derivation of band structures of electromagnetic wave'," *J. Appl. Phys.* Vol. 101, 073304, 2007; *J. Appl. Phys.*, Vol. 110, 026104, 2011.
45. Kuzmiak, V. and A. A. Maradudin, "Distribution of electromagnetic field and group velocities in two-dimensional periodic systems with dissipative metallic components," *Phy. Rev. B*, Vol. 58, No. 11, 7230–7251, 1998.
46. Li, Z. Y., J. Wang, and B. Y. Gu, "Creation of partial gaps in anisotropic photonic-band-gap structures," *Phy. Rev. B*, Vol. 58, No. 7, 3721–3729, 1998.
47. Li, Y. L., Q. Z. Xue, and C. H. Du, "Two-dimensional metallic photonic crystals with point defect analysis using modified finite-difference frequency-domain method, " *J. Lightwave Technol.*, Vol. 28, 216–221, 2010.
48. Moroz, A. and C. Sommers. "Photonic band gaps of three-dimensional face-centered cubic lattices," *J. Phys.: Condens. Matt.*, Vol. 11, 997–1008, 1999.
49. Joannopoulos, J. J., R. D. Meade, and J. N. Winn, *Photonic Crystals: Molding the Flow of Light*, Princeton University Press, New Jersey, 1995.